

Article

***In Vivo* Performance of Hierarchical HRP-Crosslinked Silk Fibroin/ β -TCP Scaffolds for Osteochondral Tissue Regeneration**

Viviana P. Ribeiro^{1,2,*}, Sandra Pina^{1,2,*}, Raphael F. Canadas^{1,2},
Alain da Silva Morais^{1,2}, Carlos Vilela^{1,2,3,4,5}, Sílvia Vieira^{1,2},
Ibrahim Fatih Cengiz^{1,2}, Rui L. Reis^{1,2,6}, Joaquim M. Oliveira^{1,2,6}

¹ 3B's Research Group, I3Bs—Research Institute on Biomaterials, Biodegradables and Biomimetics of University of Minho, Headquarters of the European Institute of Excellence on Tissue Engineering and Regenerative Medicine, Avepark, Parque de Ciência e Tecnologia, Zona Industrial da Gandra, 4805-017 Barco, Guimarães, Portugal

² ICVS/3B's—PT Government Associate Laboratory, Braga/Guimarães, 4805-017, Portugal

³ Life and Health Sciences Research Institute (ICVS), School of Health Sciences, University of Minho, Barco 4805-017, Portugal

⁴ Orthopedic Department, Centro Hospitalar do Alto Ave, Guimarães, 4810-284, Portugal

⁵ Dom Henrique Research Center, Porto, 4350-415, Portugal

⁶ The Discoveries Centre for Regenerative and Precision Medicine, Headquarters at University of Minho, Avepark, 4805-017 Barco, Guimarães, Portugal

* Correspondence: Sandra Pina, Email: sandra.pina@i3bs.uminho.pt; Tel.: +351-253510933; Viviana P. Ribeiro, Email: viviana.ribeiro@i3bs.uminho.pt; Tel.: +351-253510913.

ABSTRACT

Background: Osteochondral defects (OCD) can affect the articular cartilage and subchondral bone tissues, which requires superior therapies for the simultaneous and full restoration of such structurally and biologically different tissues.

Methods: Tissue engineered OC grafts were prepared using a horseradish peroxidase (HRP) approach to crosslink silk fibroin (HRP-SF) as the articular cartilage-like layer and an underlying HRP-SF/ZnSrTCP subchondral bone-like layer (HRP-SF/dTCP), through salt-leaching/freezing-drying methodologies. *In vivo* OC regeneration was assessed by implanting the hierarchical scaffolds in rabbit critical size OC defects, during 8 weeks. A comparative analysis was performed using hierarchical OC grafts made of pure β -TCP (HRP-SF/TCP).

Results: The hierarchical scaffolds showed good integration into the host tissue and no signs of acute inflammatory reaction, after 8 weeks of implantation. The histological analyses revealed positive collagen type II and glycosaminoglycans' formation in the articular cartilage-like layer.

Open Access

Received: 24 July 2019

Accepted: 14 September 2019

Published: 18 September 2019

Copyright © 2019 by the author(s). Licensee Hapres, London, United Kingdom. This is an open access article distributed under the terms and conditions of [Creative Commons Attribution 4.0 International License](https://creativecommons.org/licenses/by/4.0/).

New bone ingrowth's and blood vessels infiltration were detected in the subchondral bone-like layers.

Conclusions: The proposed hierarchical scaffolds presented an adequate *in vivo* response with cartilage tissue regeneration and calcified tissue formation specially promoted by the ionic incorporation into the subchondral bone layer, confirming the hierarchical structures as suitable for OCD regeneration.

KEYWORDS: silk fibroin; ZnSr-tricalcium phosphate; hierarchical scaffolds; horseradish peroxidase-mediated crosslinking; rabbit critical defect; osteochondral regeneration

ABBREVIATIONS

BMP-2, bone morphogenetic protein-2; CaPs, Calcium phosphates; ECM, extracellular matrix; GAGs, glycosaminoglicans; HAp, hydroxyapatite; HRP, horseradish peroxidase; OC, Osteochondral; OCD, Osteochondral defects; SF, silk fibroin; TE, Tissue Engineering; TCP, tricalcium phosphate

INTRODUCTION

Orthopedic surgeons have been facing major limitations in the development of personalized therapies to treat and regenerate osteochondral defects (OCD). These pathologies can simultaneously affect the articular cartilage and the subchondral bone, which implies advanced technological solutions to ensure the complete restoration of the two different tissues [1]. Cartilage defects are normally irreversible, considering its limited self-healing capacity and lack of vascularization. Subchondral bone has no such limitations, however, when an OCD reaches subchondral bone it means that articular cartilage has been deeply compromised. Another possible scenario is the loss of subchondral bone density that affects the support of articular cartilage from load bearing, resulting in cartilage tissue fracture and degeneration [2]. Diseases arising from articular cartilage can derived from natural degradation or trauma-related injuries. The current methods used to treat OCD include non-surgical therapies (drugs and/or physical therapy) and surgical techniques, depending on the severity of the defect. Arthroscopy, bone marrow stimulation (microfracture), the use of autografts or allografts, and cell-based therapy with autologous chondrocytes implantation, include the most common surgical methods used to treat OCD [3,4]. However, according to the orthopedic surgeons these are palliative and temporary solutions for improving the quality of life of patients, not ensuring the complete regenerative process of the OC tissue and the healing of mature hyaline articular cartilage [5]. With this in mind, OC tissue engineering (TE) strategies come to revolutionize the field of orthopedic surgery proposing promising alternatives for OCD repair and regeneration. Most of these strategies involve the individual or combined

application of scaffolds, cells and growth factors [6]. The initially proposed OC scaffolds were homogeneous structures used to simultaneously reach the needs of articular cartilage and subchondral bone [7]. Nowadays, the development of more complex and stratified heterogeneous structures was recognized as a better solution to treat OCD considering its hierarchical structure that contain specific mechanical properties and biological composition from the top articular cartilage layer to the underlying subchondral bone layer. Another important consideration for scaffolds design relies in the interface region between the articular cartilage and subchondral bone, also called as calcified cartilage [8]. This region has been considered by many authors as an additional layer for scaffolds production due to the recognition of its intermediate properties that do not fully fit into the articular cartilage nor in the subchondral bone properties [9]. Thus, bilayered, trilayered and multilayered scaffolds have been proposed for OCD repair and regeneration since they can better mimic the native structural complexity of OC tissue. These scaffolds should also include adequate macro-/micro-porosity, in some cases with different gradients and porous orientations [10]. For that, different processing technologies have been used, including solvent casting and particulate leaching, freeze-drying, phase separation and gas foaming, in combination with a wide range of natural and/or synthetic polymers [11]. The natural polymers are the most attractive for producing hydrogel-based scaffolds due to their aqueous nature, similarities to the native ECM and biological performance. The synthetic polymers usually present superior mechanical properties but slow biodegradability and less biocompatibility with human tissues [12]. Therefore, by means of combining synthetic- and natural-based biomaterials result in significantly enhanced mechanical and biological properties being proposed as marketed products for OC regeneration, but only a few have become clinically available. For example, the monolithic trilayered scaffold MaioRegen[®] composed by graded structures of collagen and magnesium enriched hydroxyapatite (HAp) and with a cartilage-bone interface that reproduced the tidemark of native OC tissue, have shown promising results for OC defects treatment [13]. However, one study has shown the non-homogeneous repair of OC tissue in the defective areas, which compromised the reliability of the product [14]. Another example is the cell-free biphasic scaffold TruFit[®], made of a poly(lactic-co-glycolic acid)-poly(glycolic acid)/calcium-sulfate copolymer, which showed good short-term results of OCD repair in most of the patients [15,16], but in 2009 and in the following years, different reports exhibited foreign body reactions and lack of bone ingrowth, being then removed from the market in 2013 [17,18]. The Kensey Nash Cartilage Repair Device composed of collagen type I and β -tricalcium phosphate (β -TCP)[19], and the Agili-C[™] composed of crystalline coral aragonite and hyaluronic acid [20], also include the class of cell-free bilayered scaffolds proposed to simultaneously regenerate hyaline cartilage and its underlying subchondral-bone layer.

Calcium phosphates (CaPs) are the main inorganic component of native bone tissue and the main constituent of tooth enamel, which makes them desirable for bone regeneration. Amongst CaPs, β - $(\text{Ca}_3(\text{PO}_4)_2)$ and HAp ($\text{Ca}_{10}(\text{PO}_4)_6(\text{OH})_2$), have received particular attention owing their bioactivity and biocompatibility, and ability to be gradually absorbed *in vivo* and replaced by bone over time [21]. Nevertheless, these materials are brittle bringing out poor mechanical strength particularly for load-bearing applications, which can be solved by blending them with polymers, thus combining the stiffness of CaPs with the elastic properties of the polymeric matrices to form composites with improved mechanical properties for bone applications [1,22]. Incorporating trace elements existing in bone (e.g., Sr^{2+} , Zn^{2+}) into β -TCP structure has shown enhanced growth factors like bone morphogenetic protein-2 (BMP-2) and vascular endothelial growth factor production, as well improved mechanical properties and degradation control [23,24]. Those ionic elements play an essential part in the biological action course, for example Sr^{2+} encourages bone formation and has an inhibitory role on bone resorbing osteoclast cells [25], and Zn^{2+} is an essential trace element able to promote osteoblast cell proliferation and differentiation, and has anti-angiogenic effects by decreasing the expression of genes and growth factors enrolled in angiogenesis [26].

Silk fibroin (SF) protein has attracted much attention in TE field due to the extraordinary *in vivo* biocompatibility and biodegradability, as well as, excellent mechanical elasticity and flexibility [27]. It has been proposed as a biomaterial scaffold for orthopedic repair due to its fibrous structure similar to collagen type I and type II [28]. Moreover, the semi-amorphous and hydrophilic regions between the β -sheets of SF act as deposition sites of HAp nanoparticles mimicking the anionic structure of non-collagenous proteins [29]. Different studies have also reported that the SF crystalline phase can nucleate the deposition of HAp [30], and the presence of HAp blended with amorphous SF can induce conformational changes to the protein and presents superior mechanical performance [31]. Although SF protein has poor intrinsic capacities for bone regeneration, its blending with ceramic particles can not only be advantageous to improve the mechanical behavior of the biomaterials, but also to increase their osteogenic capacity in order to mimic the structure of native bone tissue.

Highly porous 3D networks have been recognized as suitable for OC applications allowing cell infiltration and extracellular matrix (ECM) formation throughout the engineered cartilage and subchondral tissues. However, in some cases, the big challenge remains to obtain these architectures with adequate structural adaptability and resilient properties, necessary for a good integration into the host OC tissue. Hydrogel-based systems have been used for TE applications, containing a high water content that improves their elastic behavior and swelling capacity. Moreover, the hydrated nature of the hydrogels resemble the natural ECM of tissues, ensuring a suitable microenvironment for cell growth and protein delivery [32]. Recently, we have proposed a new

approach using horseradish peroxidase (HRP) to crosslink SF (HRP-SF) to form macro-/micro-porous scaffolds for cartilage and OCTE applications [11,33]. The developed hierarchical scaffolds, made of HRP-SF and HRP-SF containing β -TCP doped with zinc and strontium (HRP-SF/ZnSr- β -TCP), presented adequate structural integrity, superior mechanical properties, and excellent *in vitro* cell properties, particularly for the ion-doped structures [11]. Considering those results, herein was assessed a complementary *in vivo* evaluation of such hierarchical scaffolds, using a rabbit knee critical size OCD model. We hypothesize that the spatially limited incorporation of ZnSr- β -TCP bioresorbable powder will affect the new bone ingrowth's and mineralization, in comparison to the same structures with no ion incorporation.

MATERIALS AND METHODS

Materials and Reagents

Bombyx mori cocoons were supplied by the Portuguese Association of Parents and Friends of Mentally Disabled Citizens (APPACDM, Castelo Branco, Portugal). All reagents were purchased from Sigma-Aldrich (St. Louis, MO, USA) unless otherwise indicated.

Preparation of Concentrated Aqueous SF Solution

Bombyx mori cocoons were boiled in a sodium carbonate solution (0.02 M) for 1 h to remove the glue-like protein sericin, and then rinsed thoroughly with distilled water (30 min) in order to completely extract the degumming solution. Purified silk fibroin (SF) was dissolved in a 9.3 M lithium bromide solution for 1 h at 70 °C, and dialyzed against distilled water using a benzoylated dialysis tubing (MWCO: 2 kDa) for 48 h. Afterwards, the aqueous SF solution was concentrated in a 20 wt.% poly(ethylene) glycol solution for at least 6 h. The final concentration of SF (~20 wt.%) was determined by weighting the dry product of SF solution, left at 70 °C overnight. The SF solution was stored at 4 °C until further use (Figure 1A).

Preparation of HRP-Crosslinked SF/ZnSr-Doped β -Tricalcium Phosphate Hierarchical Scaffolds

Highly concentrated SF solution was first diluted at 16 wt.% and a horseradish peroxidase (HRP)-crosslinked SF (HRP-SF) solution was prepared by mixing the SF (16 wt.%) with HRP solution (HRP type VI, 0.84 mg/mL) and hydrogen peroxide solution (H₂O₂, 0.36 wt.%; Panreac, Barcelona, Spain). Briefly, 1 mL SF, 50 μ L HRP and 65 μ L H₂O₂ (1/0.26‰/1.45‰) were mixed and used for preparing each layer of the hierarchical scaffolds. First, the subchondral bone-like layer was produced with 80/20 (w/w) ratio of HRP-SF/ZnSr-doped β -TCP and HRP-SF/undoped β -TCP, used for comparison purposes. The β -TCP powders, pure and doped with 10 mol.% of Zn + Sr, were synthesized by aqueous

precipitation, followed by milling and sieving, with an average particle size of 1–10 μm , as previously described [34]. The ZnSr- β -TCP and β -TCP powders were mixed with the HRP-SF solution and transferred into cylindrical silicone molds (9 mm inner diameter; Deltalab, Barcelona, Spain), followed by adding 2 g of granular sodium chloride low in endotoxins (EMPROVE, VWR BDH Prolabo, Briare, France) sieved at 500–1000 μm range (Analytic Sieve Shaker; AS 200 Digit, Retsch, Germany) (Figure 1A). After gelling at 37 °C in the oven, the molds were placed in distilled water and the salt extracted (porogen) during 72 h. Finally, the subchondral bone-like scaffolds were removed from the molds using a biopsy punch (8 mm inner diameter; Smith & Nephew, Forte da Casa, Portugal). The articular cartilage-like layer was produced on the top of the subchondral bone-like scaffolds, by placing the sample pieces into new silicon molds (8 mm inner diameter) covered by HRP-SF solution. Then, 2 g of granular sodium chloride low in endotoxins (500–1000 μm) were added to the solution and left at 37 °C until complete gelation. After salt-leaching process, the hierarchical scaffolds were punched (8 mm inner diameter), frozen at -80 °C and freeze-dried (Telstar Cryodos-80, Barcelona, Spain) for 7 days (Figure 1B). Monolayered HRP-SF, HRP-SF/ZnSr- β -TCP and HRP-SF/ β -TCP scaffolds were prepared in parallel for bacteria growth evaluation. The scaffolds were abbreviated as HRP-SF/dTCP for monolayered HRP-SF/ZnSr- β -TCP scaffolds, HRP-SF/TCP for monolayered HRP-SF/ β -TCP scaffolds, BdTCP for hierarchical HRP-SF|HRP-SF/dTCP scaffolds, and BTCP for hierarchical HRP-SF|HRP-SF/TCP scaffolds, according to the nomenclature previously described [11].

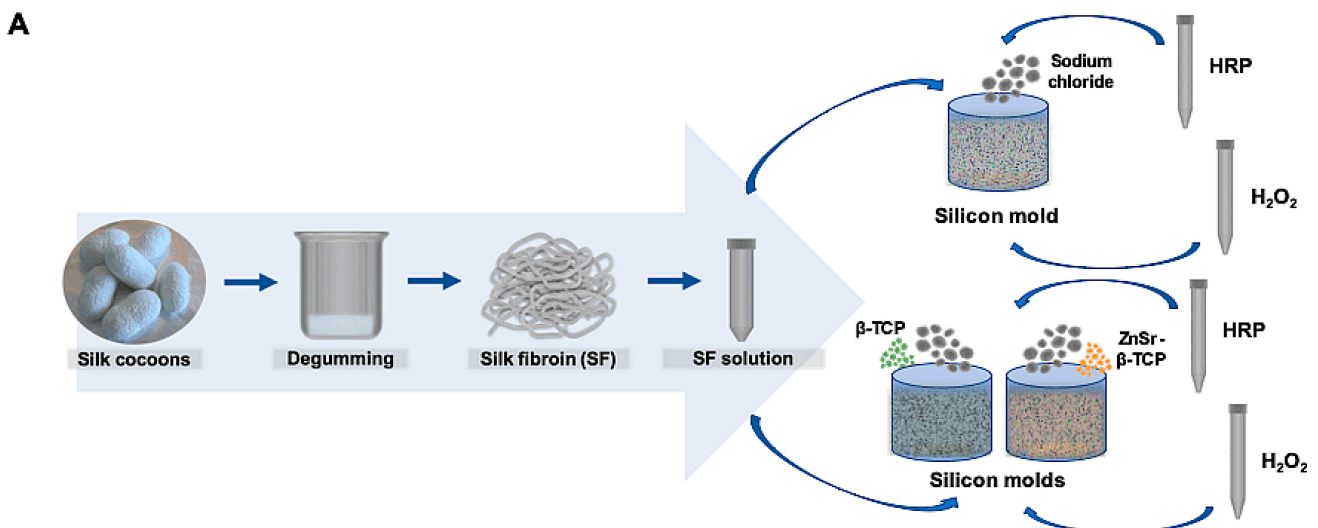


Figure 1. Schematic representation of the hierarchical scaffolds fabrication. (A) Aqueous silk fibroin (SF) extraction and purification for mixing with horseradish peroxidase (HRP) and hydrogen peroxide (H₂O₂) as crosslinking agents for preparing HRP-SF scaffolds. ZnSr- β -TCP and β -TCP particles incorporation in 80/20 (w/w) ratio of HRP-SF/ZnSr- β -TCP and HRP-SF/ β -TCP, respectively. (B) Methodology used for preparing the BdTCP and BTCP scaffolds, combining a salt-leached HRP-SF cartilage-like layer with HRP-SF/dTCP and HRP-SF/TCP subchondral bone-like layers.

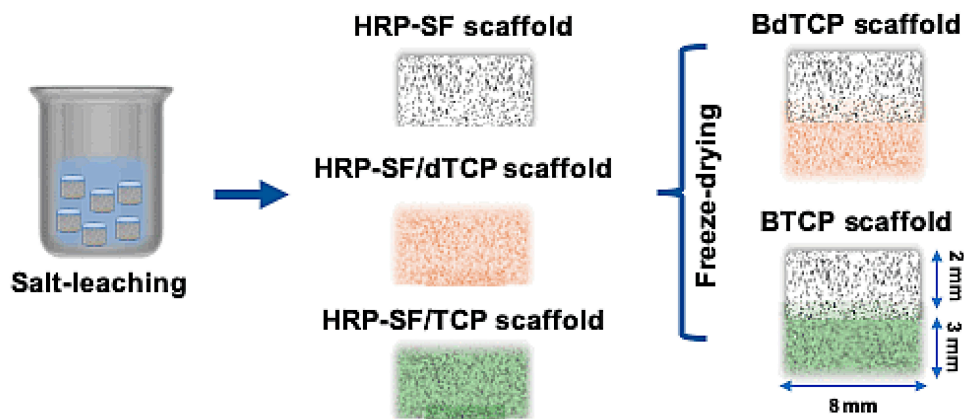
B

Figure 1. Cont.

***In vivo* Implantation of the Hierarchical Scaffolds**

The *in vivo* OC regeneration potential of the hierarchical scaffolds was evaluated by their implantation in the knee of 12 male New Zealand white rabbits (Charles River Laboratories, Saint-Germain-sur-l'Arbresle, France). All the rabbits had 11 weeks and with an average weight of 2.9 kg, at the time of implantation. All animal procedures were based upon the “3Rs” policy (Replacement, Reduction and Refinement), and their maintenance and use were performed in accordance to the European Council Directives on Animal Care (Directive 2010/63/EU) and approved by the Ethics Committee of University of Minho and by the Portuguese Licensing Authority (DGV-DSSPA) in October, 2017.

Hierarchical scaffolds of 5 mm in diameter and 5 mm in height (HRP-SF layer: 2 mm height; HRP-SF/dTCP and HRP-SF/TCP layers: 3 mm height) were used for OCD implantation. The scaffolds were previously sterilized with ethylene oxide. In total, 6 rabbits (4 critical OC defects/rabbit) were used for implanting 12 hierarchical scaffolds (6 BdTCP; 6 BTCP). The rabbits were first anesthetized using a mixture of Ketamine (25 mg/mL) and metedomidine (0.15 mL/kg), and then the hair in the knee joints of the hind legs were shaved for disinfection of the limbs. 2 OCDs (5 mm in diameter and 5 mm in depth) were created in each femur using a Brace manual drill. First, an internal para-patellar rabbit incision was performed and the patella dislocated. The drills were made located between the lateral and the medial condyle, and in the opposite site of the patellar. A press fitting technique was used for the scaffolds implantation. In each rabbit, one of the defects was empty and used as control. The rabbits were euthanized 8 weeks post-operation and the knees excised. Explants were fixed in 10% formalin for 7 days at 4 °C, decalcified in TBD-2 (Thermo Scientific, Waltham, MA, USA) at room temperature (RT) for 7 days, and analyzed by different quantitative and qualitative techniques described below.

Micro-computed tomography analysis of the explants

After fixation in formalin, the explants were analyzed by X-ray micro-computed tomography (micro-CT) before and after decalcification. The scanning of the calcified and decalcified explants was conducted using a high-resolution X-ray micro-tomography system (Skyscan 1272; Bruker, Billerica, MA, USA), with a pixel size of 15 μm , a rotation step of 0.4° over 360° , and a smoothing averaging of every 2–3 images. The acquisition parameters for bone mineral density quantification (g/cm^3) in the calcified explants were based on a calibration phantom of 10 mm diameter, and equivalent density of $0.25 \text{ g}/\text{cm}^3$ and $0.75 \text{ g}/\text{cm}^3$. The X-ray source was fixed at 80 keV and 125 μA for the calcified explants, and the decalcified explants were scanned under 50 keV and 200 μA . The specimens were reconstructed from greyscale X-ray images using NRecon (version 1.7.1.0, Bruker, Billerica, MA, USA). The samples were vertically aligned for the analysis of proximal and distal regions using DataViewer software (version 1.5.3.6, Bruker, Billerica, MA, USA). Qualitative visualization of the 3D morphology and the different phases of the BdTCP and BTCP constructs were performed using CT-Vox software (version 3.3.0, Bruker, Billerica, MA, USA). In each specimen, a cylindrical model region of interest (5 mm in diameter and 5 mm in height) was used for the quantitative evaluation in the defects implanted with the hierarchical scaffolds, defect control and healthy control, performed using a CT Analyser (version 1.17.0.0, Bruker, Billerica, MA, USA). The top 1 mm region in the cylindrical model was attributed to the articular cartilage domain (0.5 mm to cartilage; 0.5 mm to calcified cartilage), and the 4 mm in the region down were considered as subchondral bone domain, according to the thickness of normal articular cartilage and subchondral bone in rabbit knees. Soft and hard tissue content was assessed applying a threshold respectively of, 25–60 and 60–255.

Histology and immunofluorescence staining of the explants

The decalcified explants were dehydrated through increasing ethanol concentrations, and finally embedded in paraffin. All specimens were sectioned with 5 μm thick using a microtome (Spencer 820, American Optical Company, NY, USA). The obtained sections were stained with haematoxylin and eosin (H&E; Thermo Scientific, Waltham, MA, USA) to evaluate tissue distribution within the constructs layers, Masson's trichrome (Bio-Optica staining kit, Milan, Italy) to detect collagen content, and Safranin-O (0.1% v/v; Honeywell Fluka, Morris Plains, NJ, USA) to detect glycosaminoglycan's (GAGs) formation and distribution in the articular cartilage layer. For Safranin-O staining, sections were counterstained with Gill-2 haematoxylin (Thermo Scientific, Waltham, MA, USA) and Fast green (0.02% v/v; Honeywell Fluka, Morris Plains, NJ, USA).

To detect collagen type II protein expression, a monoclonal mouse anti-rabbit collagen type II alpha 1 chain-purified (Col II; Acris Antibodies GmbH, Herford, Germany) primary antibody was used following the protocol provided by the supplier. Briefly, after deparaffination and rehydration of the slides, antigen retrieval was performed by incubating slides in 0.5% pepsin in 5 mM HCl (Fisher Scientific, Waltham, MA, USA) for 45 min at 37 °C, and then the endogenous peroxidases were inactivated by using 3% (v/v) H₂O₂ solution. For Col II immunofluorescence staining, the specimens slides were incubated overnight at 4 °C with the primary antibody (dilution 1:50). Then, the slides were incubated with the respective secondary fluorochrome-conjugated antibody Alexa Fluor 594 donkey anti-mouse IgG (Invitrogen, Life Technologies, California, USA; dilution 1:100). The nuclei of the cells were counterstained with 4,6-diamidino-2-phenylindole (DAPI; Biotium, CA, USA; dilution 1:500) solution for 30 min. Slides incubated only with the secondary fluorochrome-conjugated antibody were used as negative control.

A transmitted and reflected light microscope (Axio Imager Z1 m; Zeiss, Jena, Germany) was used for histological and immunofluorescent (Col type II in red, ex/em 594/618; DAPI in blue, ex/em 358/461) analysis. Images were obtained using the Zen microscope software (Zeiss, Jena, Germany), connected to the digital cameras AxioCam MRc5 and MR3 (Zeiss, Jena, Germany).

Statistical Analysis

All the numerical results are presented as mean ± standard deviation (SD). Statistical analysis was performed using the GraphPad Prism 5.0 software (GraphPad Software, La Jolla, CA, USA), where a Shapiro-Wilk normality test was first performed to ascertain the data normality. The results indicated that a non-parametric test should be applied for quantitative micro-CT results, being therefore analyzed by means of a Mann-Whitney test, and carried out with at least 3 replicates for each condition.

RESULTS

Regeneration of Rabbit Knee OCD by the Hierarchical Scaffolds

Integration and OC tissue formation on the hierarchical scaffolds

The potential of the BdTCP and BTCP scaffolds to regenerate OCD was assessed by implanting the structures up to 8 weeks into OCD induced in rabbit knees. From the macroscopic images (Figure 2A), it can be observed that the scaffolds were well integrated into the host tissue with no signs of infection. The defect control showed regenerated tissue and no signs of adjacent collapsed tissue. The 2D cross-sections and 3D reconstructions of the explants obtained from micro-CT analysis, confirmed that the hierarchical scaffolds presented a regular morphology filling the defect area. It was observed cartilage tissue formation in the surface area of the

implants, and trabecular subchondral bone tissue presented in the bottom domain of the scaffolds, as compared to the defect control. Although from the 3D reconstructions it is not distinguishable if the calcified component (red) belongs to the TCP in the scaffolds or to the calcified tissue in the new bone, based on the scanning parameters (high voltage) chosen for these assays and on the calcified component also identified in the native subchondral bone tissue of the rabbit models (white arrows), we believe that a high amount of the detected CaP may come from the newly formed subchondral bone. The quantitative micro-CT data showed that the BdTCP scaffolds presented no significant differences of the mean porosity (Figure 2B) and mean trabecular thickness (Figure 2C), in comparison to the healthy control. On the contrary, the defect control and BTCP scaffolds presented a mean porosity (* P -value = 0.0121 and † P -value = 0.0357) and mean trabecular thickness (^ P -value = 0.0121) significantly lower than that of the healthy control. The pore size distribution showed that the BdTCP scaffolds were empty in the bottom region of the subchondral trabecular bone, similarly to the healthy control, and were gradually filled by the tissue until the top articular cartilage region. The defect control and BTCP scaffolds showed <2 mm mean pore size in the analyzed region. The defects implanted with the hierarchical scaffolds presented a higher bone mineral density (BMD) in the subchondral bone region, corresponding to the HRP-SF/dTCP and HRP-SF/TCP layers, which decreased in the articular cartilage region of the HRP-SF layers. The healthy control showed a large BMD in the subchondral bone plate and calcified cartilage, corresponding to the areas of higher bone mineral density and lower porosity in the native OC tissue of the rabbit models.

The profile of tissue distribution along the defects implanted with BdTCP scaffolds (Figure 3A), BTCP scaffolds (Figure 3B), healthy control (Figure 3C), and defect control (Figure 3D), showed an increase of the tissue filled from the trabecular bone region to the calcified cartilage region. The subchondral bone region of the defects implanted with BdTCP scaffolds was filled by hard and soft tissue at similar levels, while the articular cartilage region showed higher soft tissue distribution. Such behavior was not observed on the remaining conditions, presenting higher soft tissue content distributed along the analyzed region. Compared to the healthy control, the implanted defects and the defect control showed higher tissue regeneration in the subchondral bone region.

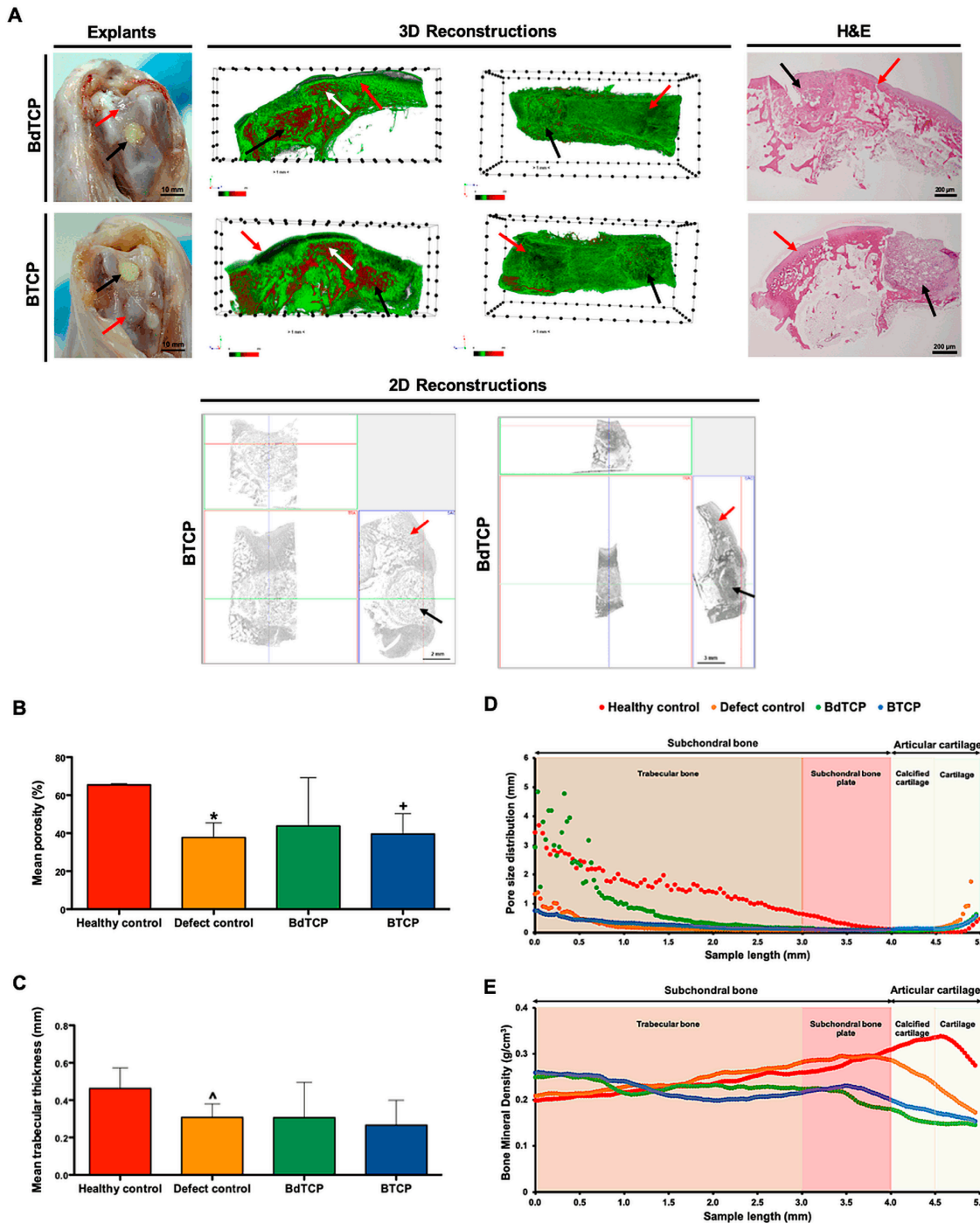


Figure 2. Structural characterization of the explants after implantation in rabbit knee OCD for the period of 8 weeks. (A) Macroscopic images, micro-CT 3D reconstructions and 2D cross-sections (transversal view in 3 different axis), and H&E staining of the explants. The black arrows indicate the implanted BdTCP and BTCP scaffolds, the red arrows indicate the defect control, and the white arrows indicate native subchondral bone tissue in the rabbit models. (B) Mean porosity, (C) mean trabecular thickness, and profiles of (D) pore size distribution, and (E) bone mineral density distribution along the pre-defined subchondral bone region and articular cartilage region of interest in the defects implanted with BdTCP scaffolds, defects implanted with BTCP scaffolds, healthy control, and defect control. Mean porosity and mean trabecular thickness data expressed as mean ± standard deviation (SD). *,+,^ Statistically significant when compared with healthy control (* *P*-value = 0.0121; + *P*-value = 0.0357; ^ *P*-value = 0.0121). Healthy control (*n* = 3); Defect control (*n* = 8); BdTCP and BTCP (*n* = 5).

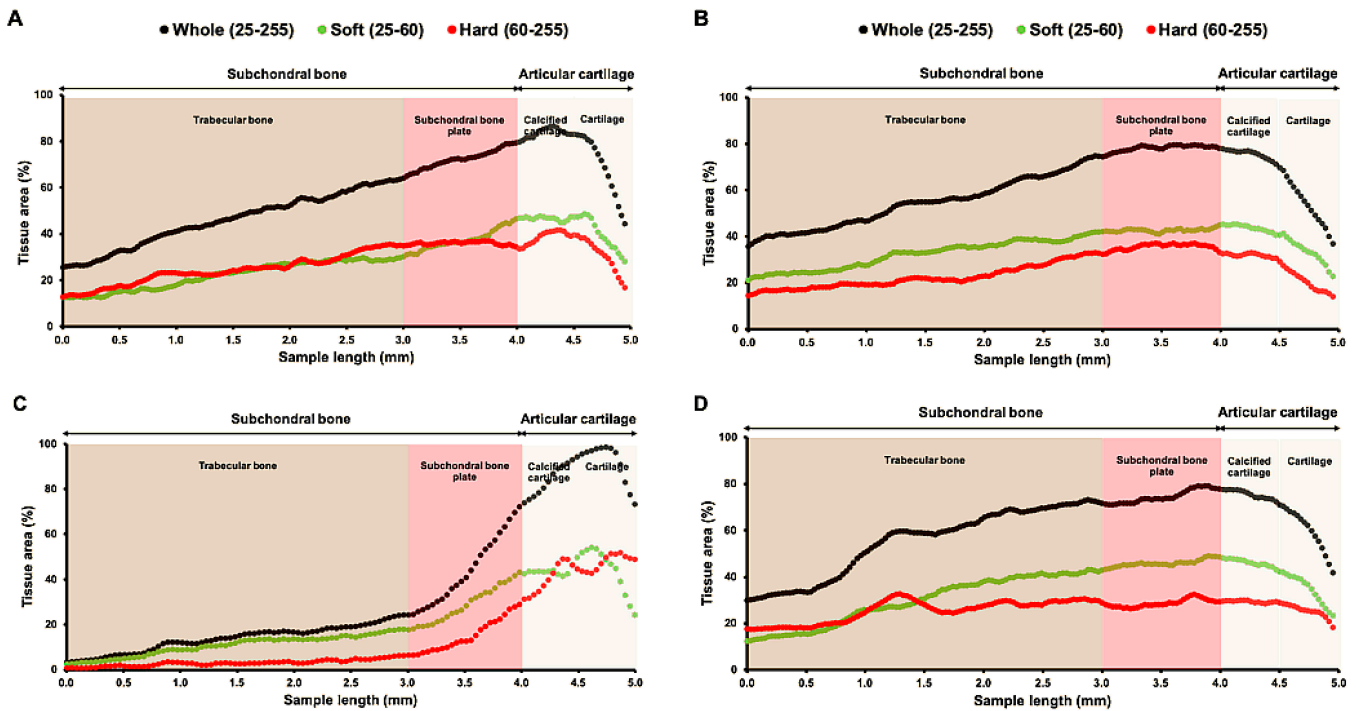


Figure 3. Profiles of soft, hard and whole tissue distribution along the pre-defined subchondral bone region and articular cartilage region of interest in the (A) defects implanted with BdTCP scaffolds, (B) defects implanted with BTCP scaffolds, (C) healthy control, and (D) defect control.

Histological characterization and immunodetection of neocartilage-forming protein

The explants were further evaluated by Masson’s trichrome and Safranin-O staining to identify the collagen deposition and the new bone tissue, as well as, GAGs formation at the newly formed ECM, respectively (Figure 4). It was possible to confirm that the implanted hierarchical scaffolds were well integrated and presented structural stability within the newly formed tissues. From Masson’s trichrome staining images (Figure 4A,B), it was found collagen deposition and a thick new cartilage layer surrounding the porous structures of the top HRP-SF layers, especially on the BdTCP scaffolds. The chondrocytes in the neocartilage tissue presented a typical round morphology. In the bottom domain, new subchondral bone growth and blood vessels infiltration were observed within the HRP-SF/dTCP (Figure 4D) and HRP-SF/TCP (Figure 4E) porous structures, which shows a good integration of the scaffolds in the host tissue. Moreover, the infiltration of the new bone was limited to the subchondral bone-like layers. The defect control also showed cartilage regeneration (Figure 4C) and new bone formation (Figure 4F), however the presence of void spaces in this region reflected some instability of the newly formed tissue (Figure 4F,L). From Safranin-O staining, it can be confirmed the formation of neocartilage tissue on the top region of the BdTCP and BTCP scaffolds, by the presence of a GAGs matrix extended into the porous HRP-SF layers (Figure 4G,H). As expected, the bottom HRP-SF/dTCP (Figure 4J) and HRP-SF/TCP (Figure 4K) layers showed no positive

staining for GAGs, indicating that the formation of new cartilage was exclusively to the top cartilage-like layers. The defect control also presented positive staining for GAGs (Figure 4I), however the formed cartilage matrix was randomly distributed. From H&E staining (Figure 4M,N), large blood vessels infiltration are easily identified as indicated by the yellow arrows.

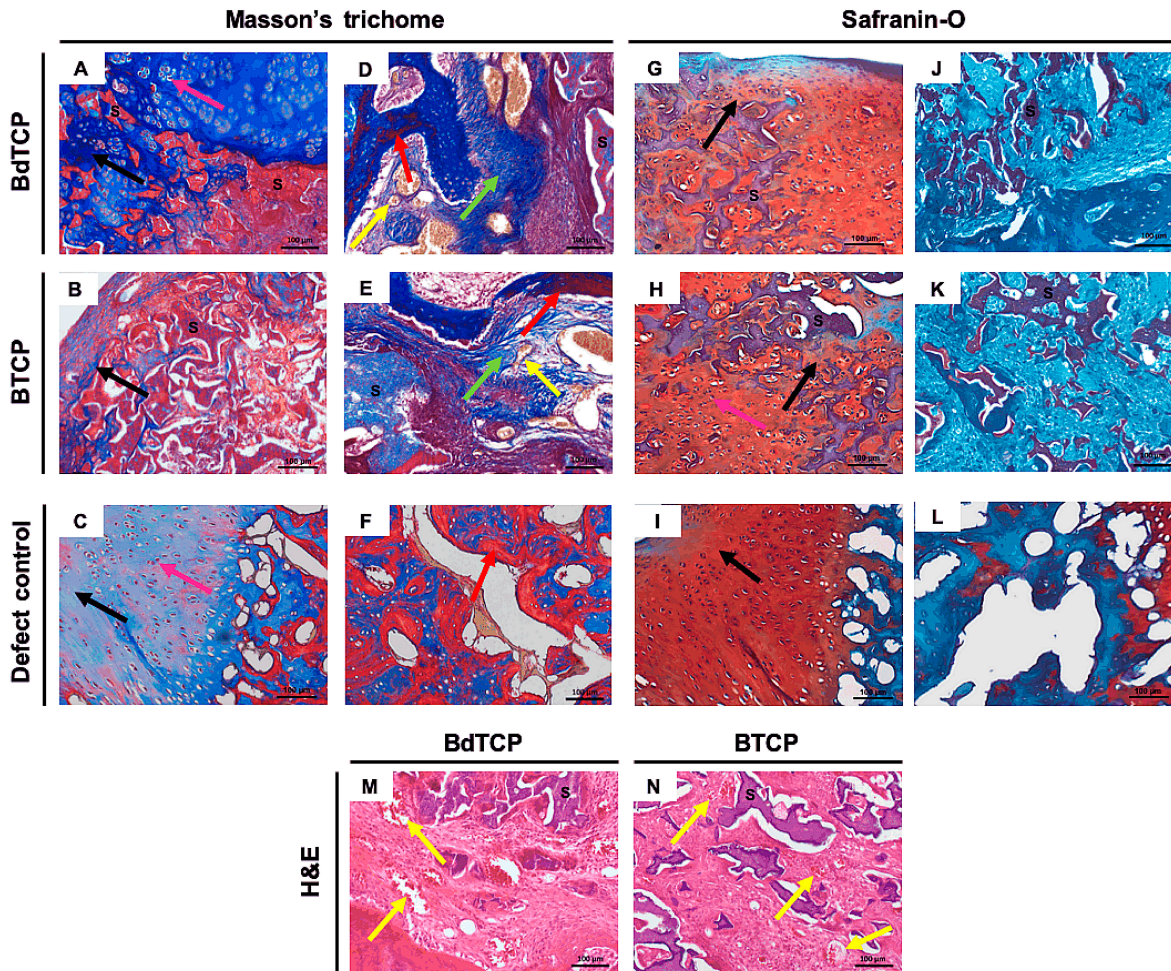


Figure 4. Histological analysis of the explants after implantation in rabbit knee OCD for 8 weeks. (A–F) Masson’s trichrome and (G–L) Safranin-O staining of the longitudinal sections of the explants. Masson’s trichrome staining of the explants in the (A–C) cartilage region and in the (D–F) subchondral bone region of the (A,B,D,E) implanted and (C,F) defect control. Safranin-O staining of the explants in the (G–I) cartilage region and in the (J–L) subchondral bone region of the (G,H,J,K) implanted and (I,L) defect control. (M,N) H&E staining of the explants in the subchondral bone region of the BdTCP and BTCP scaffolds. The black arrows indicate collagen (blue) and GAG’s (red) deposition in neocartilage tissue formation and infiltration within the HRP-SF layers of the BdTCP and BTCP scaffolds. The pink arrows indicate chondrocytes. The red arrows indicate new bone tissue (red) formation surrounded by immature fibrous connective tissue (blue; green arrows). The yellow arrows indicate blood vessels (orange). “S” indicates stained scaffolds (HRP-SF, HRP-SF/dTCP, and HRP-SF/TCP).

From Col II immunofluorescence analysis, the formation of neocartilage tissue inside the porous HRP-SF layers of the BdTCP

(Figure 5A) and BTCP (Figure 5B) scaffolds was confirmed. The defect control also showed positive staining of Col II (Figure 5C).

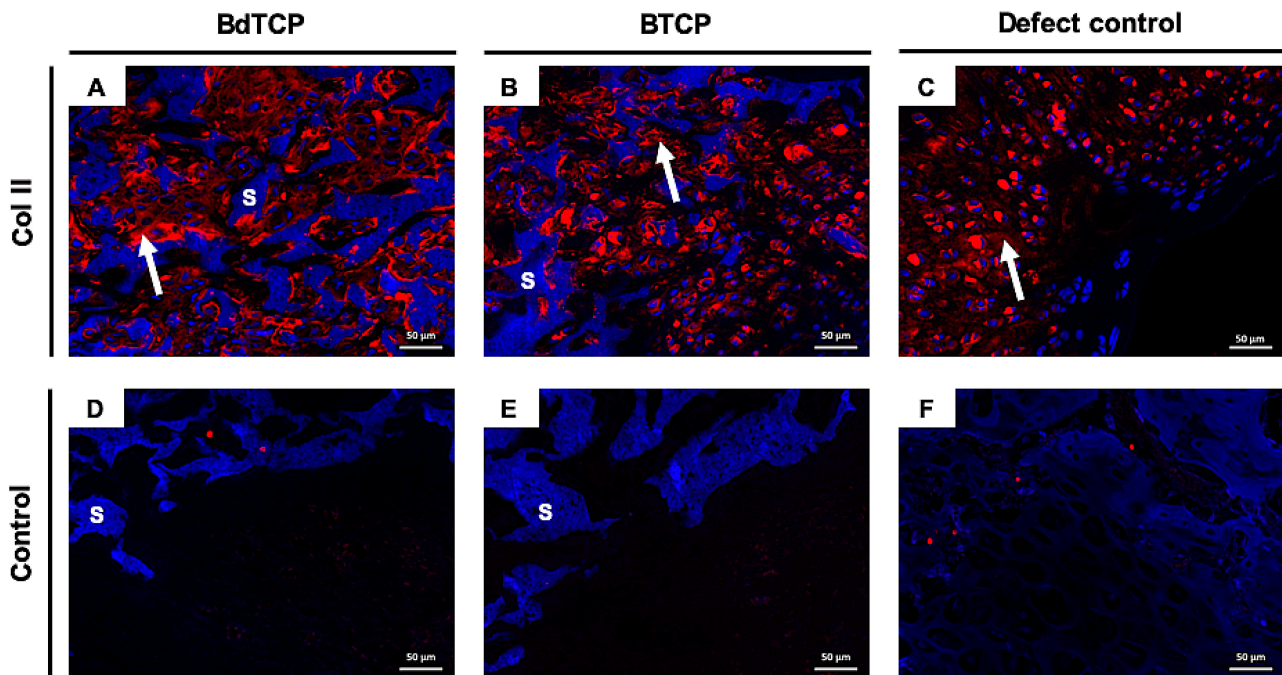


Figure 5. Col II immunofluorescence analysis of the explants. (A–C) Col II staining for the neocartilage formed in the HRP-SF layer of the BdTCP and BTCP scaffolds, and in the surface area of the defect control, respectively. (D–F) Negative control for A–C, respectively. In representative immunofluorescence images, the nuclei are stained in blue and Col II is stained in red. “S” indicates HRP-SF scaffolds autofluorescence in blue, and the white arrows indicate Col II in the regenerated cartilage.

DISCUSSION

OC tissue regeneration remains a big challenge for TE researchers and orthopedic surgeons. The high complexity of OC tissue relies in its dual structural, biochemical and cellular composition. In the avascular chondral layer reside chondrocytes, surrounded by a highly aqueous ECM composed by collagen type II and proteoglycans. On the other side, a highly vascularized subchondral bone layer is composed by different types of cells (e.g., bone marrow cells, osteoblasts, osteocytes and osteoclasts), collagen type I and the inorganic phase HAp [7]. Thus, when considering a scaffold as an innovative strategy to OCD treatment, different features should be considered. It has been recognized that bilayered scaffolds composed by specific mechanical, chemical and morphological properties in each layer, are more likely to simultaneously satisfy the regeneration of the articular cartilage and subchondral bone tissues [1]. Moreover, advances have been made for the fabrication of an intermediate region that mimics the interface between the two layers and interconnects their distinct properties [35]. For example, Ding *et al.* [36] developed integrated OC composite scaffolds containing three layers. The top cartilage layer was made of SF presenting longitudinal orientation and microtubular structure, whereas the lower subchondral bone layer

presented a highly porous three-dimensional (3D) structure composed of SF and HAp. A dense intermediate region also composed of SF/HAp served as boundary between the chondral and subchondral bone layers. The scaffolds showed bioactivity and supported human adipose-derived stem cells differentiation towards chondrocytes and osteoblasts *in vitro*. The existence of a dense intermediate region also prevented the mixing of the cells between the chondral and the bone layers, favoring the differentiation pattern on the respective layers of the scaffolds.

Fully integrated SF/SF-nanoCaP hierarchical scaffolds were also proposed by Yan *et al.* [37] for OCD regeneration. The authors used salt-leaching/freeze-drying methodologies to form highly porous structures with homogeneous pore distribution along the scaffolds. The integration of a SF-based cartilage like layer with a SF/nano-CaP subchondral bone-like layer allowed to obtain hierarchical structures with distinct but interconnected properties. The CaP phase was only retained on the underlying subchondral bone layer (SF-nanoCaP) improving the mechanical properties of scaffolds and the osteogenic activity of rabbit bone marrow mesenchymal stromal cells. Moreover, in rabbit knee OCD, the firmly integrated scaffolds showed collagen type II positive staining and GAGs formation on the top SF layer, together with new bone ingrowth and blood vessels infiltration on the underlying SF-nanoCaP layer [38–40]. The suitability of macro-/micro-porous HRP-crosslinked SF scaffolds for cartilage TE applications was also demonstrated in our previous works [33]. These structures presented combined features of chemically and mechanically stable SF scaffolds, with the elastic behavior of enzymatically crosslinked SF hydrogels [41,42].

As aforementioned, hydrogel-based networks are attractive for building 3D structures for OC tissue regeneration, that resemble the ECM due to their high water content, viscoelastic nature, and the easy diffusion of biomacromolecules. Thus, the possibility of structuring hydrogel-based matrices in order to increase their porosity for guiding cell infiltration, orientation and ECM formation is of paramount importance for OC tissue regeneration. For example, Canadas *et al.* [43] developed a novel 3D OC tissue model made of methacrylated gellan gum blended with gelatin and produced both with linear and random porosity distribution, using temperature gradients and freeze-drying process. The porous hydrogels presented isotropic and anisotropic structures with different pore sizes and porosity according to the OC layer. It was also showed different gradient distributions using HAp micro-particles in combination with growth factors, which contributed for the formation of a heterotypic-like OC tissue with different cell orientations according to the chondral or subchondral layer. We have recently developed HRP-SF to form macro-/micro-porous scaffolds using salt-leaching/freeze-drying methodologies for cartilage TE applications [33]. The obtained structures have shown the ability to support human adipose derived stem cells, chondrogenic differentiation and cartilage-like ECM formation within the

interconnected porous matrices. Additionally, with the applied methodologies the crystallinity of SF protein increased thus improving the scaffolds mechanical properties and structural stability, as compared to pure HRP-crosslinked SF hydrogels produced with amorphous conformation [41]. On the basis of these findings, we have further developed novel hierarchical scaffolds integrating the HRP-crosslinked SF scaffolds as articular cartilage-like layer, into an underlying HRP-crosslinked SF scaffolds containing β -TCP doped with zinc and strontium (HRP-SF/ZnSr- β -TCP), as subchondral bone-like layer [11]. The scaffolds presented adequate structural integrity, homogeneous porosity distribution and the TCP phase confined to the subchondral bone-like layer. As major particularities, these structures presented resilient properties and viscoelastic nature for an easy adjustment to fill OCD. The *in vitro* biomineralization capability of the bilayered scaffolds after soaking in a simulated body fluid for 15 days, showed the formation of a cauliflower-like apatite layer, mainly due to the presence of Sr and Zn trace elements. Furthermore, *in vitro* response of co-cultured human osteoblasts and human chondrocytes showed an outstanding performance for cell adhesion, proliferation, and ECM production, owing the chemical properties of SF, the crystalline structure of β -TCP and the presence of ionic dopants. It was also observed osteogenic activity and chondrogenic inducement, respectively represented by the formation of a mineralized matrix and GAGs deposition, in the subchondral and chondral-like layers. In the interface region, the genotypic expression of Col X, as a marker of pre-hypertrophic chondrocytes, confirmed the hierarchical and stratified properties of the ion incorporation into the hierarchical scaffolds. Although worthy outcomes have been obtained so far, a complementary *in vivo* evaluation was demanded to observe the overall effects of those biofunctional structures in a living OCD. Therefore, in the present study, rabbit knee OCD were used as animal model to induce the OC regeneration potential of the hierarchical scaffolds. It was observed that the fixation of the implanted scaffolds was easy, while maintaining their dimensions over the implantation period (Figure 2A). It has been reported that the swell behavior of the scaffolds can be a problem for the implantation and in some cases, their fixation can be also compromised [44]. Herein, an expected swelling was reached in order to completely fill the empty space of the defects, however, no protrusions or signs of acute inflammatory reaction were observed. The results may be related to the resilient and viscoelastic properties of the HRP-crosslinked hierarchical scaffolds [11], which contributed to the superior structural stability. From the 3D reconstructions of the explants, the regular morphology and good stability of the scaffolds filling the defect area were confirmed, as well as, the proposed structures were able to support the cartilage tissue formation and the subchondral bone regeneration, with a high content of CaP detected in the HRP-SF/dTCP and HRP-SF/TCP layers. Confirming these observations, the BMD distribution within the subchondral bone layers of

the BdTCP and BTCP scaffolds was superior to that observed in the top of HRP-SF layers (Figure 2E). Previously, Yan *et al.* [37] showed that the good integration of SF/SF-nanoCaP porous hierarchical scaffolds in rabbit knee OCD enable a rapid subchondral bone regeneration after 4 weeks of implantation. The fast formation of new subchondral bone tissue is critical to fix the implants into the defect sites, but also to provide mechanical support for the subsequent regeneration of articular cartilage tissue [45]. The authors also observed a small amount of subchondral bone tissue in the empty defects, contrary to the high content of regenerated tissue observed in the defect controls of our study, after a longer implantation period (8 weeks). The good outcomes of the ionic presence into the hierarchical scaffolds were confirmed by the similar porosity (Figure 2B), trabecular thickness (Figure 2C), and pore size distribution (Figure 2D) of the BdTCP scaffolds to that obtained for the healthy controls. Moreover, in the subchondral bone region the BdTCP scaffolds were filled by hard and soft tissue at similar levels (Figure 3A), which indicates the strong impact of Zn and Sr elements on bone formation and mineralization, by means of improving the microstructure and crystallinity of β -TCP [34,46].

The OC tissue regeneration was further analyzed by histology and immunohistochemistry. The main indicators of articular cartilage tissue formation in OCD regeneration, are the formation of the specific hyaline cartilage components GAG's and Col II [47]. In the present study, we were able to observe the collagen deposition and GAGs matrix formation on the top HRP-SF layers of the BdTCP (Figure 4A,G) and BTCP (Figure 4B,H) scaffolds, indicating that these structures were advantageous in supporting neocartilage tissue formation. These observations were also confirmed by the cartilage-specific protein expression of Col II in this region (Figure 5A,B). The infiltration of chondrocytes and newly formed cartilage within the porous structure of the top HRP-SF layers, revealed the importance of a high and controlled porosity in cell infiltration, proliferation and ECM formation [47,48]. When observing tissue formation within the HRP-SF/dTCP (Figure 4D) and HRP-SF/TCP (Figure 4E) layers, new bone ingrowth and blood vessel infiltration were clearly observed (Figure 4M,N). The availability of good vascularization pathways is another important issue when considering a scaffold for OCD regeneration and rapid subchondral bone formation [49]. Once again, the production of highly porous structures may have contributed to the obtained results [50]. Thus, the *in vivo* results revealed that the hierarchical scaffolds support rabbit knee OCD regeneration.

CONCLUSIONS

In this study, the *in vivo* performance of hierarchical scaffolds made of HRP-SF and HRP-SF/ZnSrTCP layers respectively, as the articular cartilage-like layer and an underlying subchondral bone-like layer, was assessed using rabbit critical size OC defects. The hierarchical scaffolds presented good integration into the host tissue and no signs of acute inflammatory

reaction, after 8 weeks of implantation. Histological and immunofluorescence analyses confirmed the cartilage tissue regeneration, as observed by the presence of GAGs and collagen type II positive staining's in the HRP-SF layer. *De novo* bone ingrowth and blood vessels infiltration were also observed on the underlying HRP-SF/ZnSr- β -TCP and HRP-SF/ β -TCP layers, suggesting that the presence of inorganic ionic-doped β -TCP promoted subchondral tissue formation. Although long-term studies are needed to ensure the beneficial effect of the ionic presence, as well the implant-tissue interactions and resorption, the results herein obtained suggest that the proposed hierarchical scaffolds may be potentially used in OCD regeneration.

AUTHOR CONTRIBUTIONS

Conceptualization, VPR, RFC and SP; Methodology, VPR, RFC, ASM, CV and SV; Investigation, VPR, RFC, ASM, CV, SV and IFC; Writing – Original Draft Preparation, VPR; Writing-Review and Editing, SP, RLR and JMO. Supervision, JMO; Funding Administration, RLR and JMO. All authors agree to be accountable for the work and to ensure that any questions relating to the accuracy and integrity of the paper are investigated and properly resolved.

CONFLICTS OF INTEREST

The authors declare that they have no conflicts of interest.

FUNDING

This research was funded by the Portuguese Foundation for Science and Technology for the Hierarchitech project (M-era-Net/0001/2014), for the fellowships (SFRH/BD/99555/2014) and (SFRH/BPD/101952/2014), and for the distinctions attributed to JMO (IF/01285/2015) and SP (CEECIND/03673/2017). Also, financial support from FCT/MCTES (Fundação para a Ciência e a Tecnologia/ Ministério Da Ciência, Tecnologia, e Ensino Superior) and fundo social europeu através do programa operacional do capital humano (FSE/POCH), PD/59/2013, PD/BD/113806/2015.

ACKNOWLEDGMENTS

The authors thank to Teresa Oliveira for the assistance with the histological samples preparation and processing.

REFERENCES

1. Yousefi AM, Hoque ME, Prasad RG, Uth N. Current strategies in multiphasic scaffold design for osteochondral tissue engineering: a review. *J Biomed Mater Res A*. 2015;103(7):2460-81.
2. Madry H, Orth P, Cucchiaroni M. Role of the subchondral bone in articular cartilage degeneration and repair. *J Am Acad Orthop Surg*. 2016;24(4):e45-6.

3. Zhang W, Ouyang H, Dass CR, Xu J. Current research on pharmacologic and regenerative therapies for osteoarthritis. *Bone Res.* 2016;4:15040.
4. Devitt BM, Bell SW, Webster KE, Feller JA, Whitehead TS. Surgical treatments of cartilage defects of the knee: systematic review of randomised controlled trials. *Knee.* 2017;24(3):508-17.
5. De L'Escalopier N, Barbier O, Mainard D, Mayer J, Ollat D, Versier G. Outcomes of talar dome osteochondral defect repair using osteochondral autografts: 37 cases of Mosaicplasty®. *Orthop Traumatol Surg Res.* 2015;101(1):97-102.
6. Mendes L, Katagiri H, Tam W, Chai Y, Geris L, Roberts S, et al. Advancing osteochondral tissue engineering: bone morphogenetic protein, transforming growth factor, and fibroblast growth factor signaling drive ordered differentiation of periosteal cells resulting in stable cartilage and bone formation *in vivo*. *Stem Cell Res Ther.* 2018;9(1):42.
7. Nukavarapu SP, Dorcemus DL. Osteochondral tissue engineering: current strategies and challenges. *Biotechnol Adv.* 2013;31(5):706-21.
8. Kosik-Kozioł A, Costantini M, Mróz A, Idaszek J, Heljak M, Jaroszewicz J, et al. 3D bioprinted hydrogel model incorporating β -tricalcium phosphate for calcified cartilage tissue engineering. *Biofabrication.* 2019;11(3):035016.
9. Di Luca A, Van Blitterswijk C, Moroni L. The osteochondral interface as a gradient tissue: From development to the fabrication of gradient scaffolds for regenerative medicine. *Birth Defects Res C Embryo Today.* 2015;105(1):34-52.
10. Kang H, Zeng Y, Varghese S. Functionally graded multilayer scaffolds for *in vivo* osteochondral tissue engineering. *Acta Biomater.* 2018;78:365-77.
11. Ribeiro VP, Pina S, Costa JB, Cengiz IF, García-Fernández L, Fernández-Gutiérrez MDM, et al. Enzymatically Cross-Linked Silk Fibroin-Based Hierarchical Scaffolds for Osteochondral Regeneration. *ACS Appl Mater Interfaces.* 2019;11(4):3781-99.
12. Stratton S, Shelke NB, Hoshino K, Rudraiah S, Kumbar SG. Bioactive polymeric scaffolds for tissue engineering. *Bioact Mater.* 2016;1(2):93-108.
13. Christensen BB, Foldager CB, Jensen J, Jensen NC, Lind M. Poor osteochondral repair by a biomimetic collagen scaffold: 1-to 3-year clinical and radiological follow-up. *Knee Surg Sports Traumatol Arthrosc.* 2016;24(7):2380-7.
14. Filardo G, Kon E, Di Martino A, Busacca M, Altadonna G, Marcacci M. Treatment of knee osteochondritis dissecans with a cell-free biomimetic osteochondral scaffold: clinical and imaging evaluation at 2-year follow-up. *Am J Sports Med.* 2013;41(8):1786-93.
15. Davidson PA, Rivenburgh DW. Prospective evaluation of osteochondral defects in the knee treated with biodegradable scaffolds (SS-45). *Arthroscopy.* 2007;23(6):e22-3.
16. Bekkers JE, Bartels LW, Vincken KL, Dhert WJ, Creemers LB, Saris DB. Articular cartilage evaluation after TruFit plug implantation analyzed by delayed gadolinium-enhanced MRI of cartilage (dGEMRIC). *Am J Sports Med.* 2013;41(6):1290-5.
17. Carmont MR, Carey-Smith R, Saithna A, Dhillon M, Thompson P, Spalding T. Delayed incorporation of a TruFit plug: perseverance is recommended. *Arthroscopy.* 2009;25(7):810-4.

18. Barber FA, Dockery WD. A computed tomography scan assessment of synthetic multiphase polymer scaffolds used for osteochondral defect repair. *Arthroscopy*. 2011;27(1):60-4.
19. Canadas RF, Pina S, Marques AP, Oliveira JM, Reis RL. Cartilage and bone regeneration: how close are we to bedside? *Stem Cells Transl Med*. 2017;6(12):2186-96.
20. Kon E, Filardo G, Perdisa F, Venieri G, Marcacci M. Clinical results of multilayered biomaterials for osteochondral regeneration. *J Exp Orthop*. 2014;1(1):10.
21. Pina S, Rebelo R, Correlo VM, Oliveira JM, Reis RL. Bioceramics for Osteochondral Tissue Engineering and Regeneration. *Adv Exp Med Biol*. 2018;1058:53-75.
22. Liang X, Duan P, Gao J, Guo R, Qu Z, Li X, et al. Bilayered PLGA/PLGA-HAP composite scaffold for osteochondral tissue engineering and tissue regeneration. *ACS Biomater Sci Eng*. 2018;4(10):3506-21.
23. Bose S, Fielding G, Tarafder S, Bandyopadhyay A. Understanding of dopant-induced osteogenesis and angiogenesis in calcium phosphate ceramics. *Trends Biotechnol*. 2013;31(10):594-605. doi: 10.1016/j.tibtech.2013.06.005
24. Fielding G, Bose S. SiO₂ and ZnO Dopants in 3D Printed TCP Scaffolds Enhances Osteogenesis and Angiogenesis *in vivo*. *Acta Biomater*. 2013;9(11):9137-48. doi: 10.1016/j.actbio.2013.07.009
25. Saidak Z, Marie PJ. Strontium signaling: Molecular mechanisms and therapeutic implications in osteoporosis. *Pharmacol Ther*. 2012;136(2):216-26.
26. Kandaz M, Ertekin MV, Erdemci B, Kızıltunç A, Koçer İ, Özmen HK, et al. The Effects of Zinc Sulfate on the Levels of Some Elements and Oxidative Stress Occurring in Lenses of Rats Exposed to Total Cranium Radiotherapy. *Eurasian J Med*. 2009;41(2):110-5.
27. Melke J, Midha S, Ghosh S, Ito K, Hofmann S. Silk fibroin as biomaterial for bone tissue engineering. *Acta Biomater*. 2016;31:1-16.
28. Wang X, Kim HJ, Wong C, Vepari C, Matsumoto A, Kaplan DL. Fibrous proteins and tissue engineering. *Mater Today*. 2006;9(12):44-53.
29. Marelli B, Ghezzi CE, Alessandrino A, Barralet JE, Freddi G, Nazhat SN. Silk fibroin derived polypeptide-induced biomineralization of collagen. *Biomaterials*. 2012;33(1):102-8.
30. Vetsch JR, Paulsen SJ, Müller R, Hofmann S. Effect of fetal bovine serum on mineralization in silk fibroin scaffolds. *Acta Biomater*. 2015;13:277-85.
31. Jin Y, Kundu B, Cai Y, Kundu SC, Yao J. Bio-inspired mineralization of hydroxyapatite in 3D silk fibroin hydrogel for bone tissue engineering. *Colloids Surf B Biointerfaces*. 2015;134:339-45.
32. Lee J-H, Kim H-W. Emerging properties of hydrogels in tissue engineering. *J Tissue Eng*. 2018;9:2041731418768285.
33. Ribeiro VP, da Silva Morais A, Maia FR, Canadas RF, Costa JB, Oliveira AL, et al. Combinatory approach for developing silk fibroin scaffolds for cartilage regeneration. *Acta Biomater*. 2018;72:167-81.

34. Pina S, Canadas R, Jiménez G, Perán M, Marchal J, Reis R, et al. Biofunctional ionic-doped calcium phosphates: silk fibroin composites for bone tissue engineering scaffolding. *Cells Tissues Organs*. 2017;204(3-4):150-63.
35. Lu HH, Subramony SD, Boushell MK, Zhang X. Tissue engineering strategies for the regeneration of orthopedic interfaces. *Ann Biomed Eng*. 2010;38(6):2142-54.
36. Ding X, Zhu M, Xu B, Zhang J, Zhao Y, Ji S, et al. Integrated trilayered silk fibroin scaffold for osteochondral differentiation of adipose-derived stem cells. *ACS Appl Mater Interfaces*. 2014;6(19):16696-705.
37. Yan LP, Silva-Correia J, Oliveira MB, Vilela C, Pereira H, Sousa RA, et al. Bilayered silk/silk-nanoCaP scaffolds for osteochondral tissue engineering: *In vitro* and *in vivo* assessment of biological performance. *Acta Biomater*. 2015;12:227-41.
38. Yan L-P, Oliveira JM, Oliveira AL, Caridade SG, Mano JF, Reis RL. Macro/microporous silk fibroin scaffolds with potential for articular cartilage and meniscus tissue engineering applications. *Acta Biomater*. 2012;8(1):289-301.
39. Yan L-P, Silva-Correia J, Correia C, Caridade SG, Fernandes EM, Sousa RA, et al. Bioactive macro/micro porous silk fibroin/nano-sized calcium phosphate scaffolds with potential for bone-tissue-engineering applications. *Nanomedicine*. 2013;8(3):359-78.
40. Yan L-P, Salgado AJ, Oliveira JM, Oliveira AL, Reis RL. De novo bone formation on macro/microporous silk and silk/nano-sized calcium phosphate scaffolds. *J Bioact Compat Polym*. 2013;28(5):439-52.
41. Yan L-P, Silva-Correia J, Ribeiro VP, Miranda-Gonçalves V, Correia C, da Silva Morais A, et al. Tumor growth suppression induced by biomimetic silk fibroin hydrogels. *Sci Rep*. 2016;6:31037.
42. Ribeiro VP, Silva-Correia J, Gonçalves C, Pina S, Radhouani H, Montonen T, et al. Rapidly responsive silk fibroin hydrogels as an artificial matrix for the programmed tumor cells death. *PLoS One*. 2018;13(4):e0194441.
43. Canadas RF, Ren T, Marques AP, Oliveira JM, Reis RL, Demirci U. Biochemical Gradients to Generate 3D Heterotypic-Like Tissues with Isotropic and Anisotropic Architectures. *Adv Funct Mater*. 2018;28(48):1804148.
44. Kon E, Delcogliano M, Filardo G, Busacca M, Di Martino A, Marcacci M. Novel nano-composite multilayered biomaterial for osteochondral regeneration: a pilot clinical trial. *Am J Sports Med*. 2011;39(6):1180-90.
45. Gomoll AH, Madry H, Knutsen G, van Dijk N, Seil R, Brittberg M, et al. The subchondral bone in articular cartilage repair: current problems in the surgical management. *Knee Surg Sports Traumatol Arthrosc*. 2010;18(4):434-47.
46. Jiménez M, Abradelo C, San Román J, Rojo L. Bibliographic review on the state of the art of strontium and zinc based regenerative therapies. Recent developments and clinical applications. *J Mater Chem B*. 2019;7(12):1974-85.
47. Wang Y, Kim U-J, Blasioli DJ, Kim H-J, Kaplan DL. *In vitro* cartilage tissue engineering with 3D porous aqueous-derived silk scaffolds and mesenchymal stem cells. *Biomaterials*. 2005;26(34):7082-94.

48. Lien S-M, Ko L-Y, Huang T-J. Effect of pore size on ECM secretion and cell growth in gelatin scaffold for articular cartilage tissue engineering. *Acta Biomater.* 2009;5(2):670-9.
49. Fuchs S, Jiang X, Schmidt H, Dohle E, Ghanaati S, Orth C, et al. Dynamic processes involved in the pre-vascularization of silk fibroin constructs for bone regeneration using outgrowth endothelial cells. *Biomaterials.* 2009;30(7):1329-38.
50. Mercado-Pagán ÁE, Stahl AM, Shanjani Y, Yang Y. Vascularization in bone tissue engineering constructs. *Ann Biomed Eng.* 2015;43(3):718-29.

How to cite this article:

Ribeiro VP, Pina S, Canadas RF, da Silva Morais A, Vilela C, Vieira S, et al. *In Vivo* Performance of Hierarchical HRP-Crosslinked Silk Fibroin/ β -TCP Scaffolds for Osteochondral Tissue Regeneration. *Regen Med Front.* 2019;1:e190007. <https://doi.org/10.20900/rmf20190007>